THE JOURNAL OF PHYSICAL CHEMISTRY C

Article

pubs.acs.org/JPCC

Biomorph Oscillations Self-organize Micrometer-Scale Patterns and Nanorod Alignment Waves

Elias Nakouzi, Yara E. Ghoussoub, Pamela Knoll, and Oliver Steinbock*

Department of Chemistry and Biochemistry, Florida State University, Tallahassee, Florida 32306-4390, United States

Supporting Information

ABSTRACT: The coprecipitation of barium carbonate and silica spontaneously creates complex micrometer-scale objects such as sheets and helices. These structures consist of densely packed crystalline nanorods that in the case of sheets align in radial direction. We report the existence of an additional level of self-organization that creates oscillatory height variations in biomorph sheets. These topographic features take the form of either concentric rings or disordered, patchy patterns and form immediately in the wake of the crystallization front. Their wavelength varies around 6.5 μm and shows no pronounced dependence on the reactant concentrations. Atomic force microscopy reveals height variations of up to 500 nm which equal 45% of the average sheet thickness. These undulations are accompanied by a systematic out-of-plane displacement of the nanorods. Our results are discussed in the context of an earlier hypothesis that predicts pH oscillations near the crystallization front.

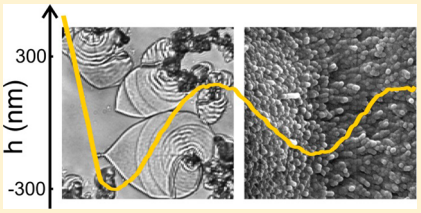

INTRODUCTION

One of the great opportunities for modern materials science is the use of nonequilibrium conditions for the design of systems that self-assemble complex, functional structures.[1] This approach has the potential to replace conventional, serial lithography techniques with highly efficient, parallel bottom-up strategies. Recent advances toward this goal include the synthesis of functionalized meso-structures,[2−5] hybrid materials,[6−8] catalytic nanodendrites,[9,10] self-propelled particles,[11,12] and self-healing polymers.[13,14] Also, natural biomineralization provides striking examples for the emergence of structural complexity from dynamic chemical environments.[15] For instance, mollusk shells form multiscale morphological features in response to chemical variations at the growth front. The resulting hierarchical architectures impart the shells with performance properties that cannot be accessed by classical crystallization. It is hence not surprising that significant efforts have been made to understand and reproduce biomimetic crystallization pathways for the production of bioinspired materials.[16−18]

An important model for studying the bottom-up assembly of complex materials is the coprecipitation of silica and barium carbonate in alkaline media.[19−24] In this system, the simple diffusion of atmospheric carbon dioxide into the reaction solution prompts the formation of elaborate polycrystalline microstructures known as biomorphs. Interestingly, these purely inorganic aggregates assemble life-like morphologies such as cardioid leaves, curved worms, and helical filaments.[25−27] Recent hypotheses on the growth mechanism are based on the solubility trends of barium carbonate and silica in different pH environments.[28,29] Specifically, the nucleation of barium carbonate nanocrystals decreases the local pH which causes the precipitation of amorphous silica. The resulting pH increase at the growth interface induces the deposition of further carbonate crystallites. During each cycle of the oscillatory process, the carbonate nanorods are cemented into an amorphous silica framework. Although some experimental observations have provided indirect support for this mechanism,[30−32] no direct evidence for the chemical oscillations has been reported yet. In this study, we document and characterize periodic modulations in the biomorph structure that unambiguously arise in an oscillatory fashion. Faint evidence for the oscillations was seen earlier reports, but these features were neither studied nor acknowledged.[24,26,28] Last, we discuss the implications of our findings for the validity of the pH oscillation model.

EXPERIMENTAL METHODS

Silica−carbonate biomorphs are deposited from 4 mL solutions of $[BaCl_2]$ = 5 mM and $[Na_2SiO_3]$ = 8.4 mM in Greiner Bio-One Petri dishes with 3.5 cm diameters. The average height of the crystallization solutions is thus 0.42 cm. After adding the reactants, we adjust the pH to 10.2−10.6 by adding 3−5 drops of 0.1 M HCl and mix the solution. The biomorph structures form spontaneously over a period of 8−10 h and are observed using a Nikon Elements Ti inverted microscope equipped with a Photometrics Coolsnap HQ2 charge-coupled device camera. Time-lapse imaging of the biomorph growth is controlled by the NIS Elements software package. For the instrumental analyses, the biomorph structures are grown on rectangular glass slides. The substrates are retrieved, rinsed, and dried after the crystal aggregates grow to their mature biomorphic shapes.

The samples are subsequently coated with thin Au films in preparation for electron microscopy analysis. A Zeiss 1540EsB

Received: May 7, 2015
Revised: June 3, 2015
Published: June 8, 2015

DOI: 10.1021/acs.jpcc.5b04411
J. Phys. Chem. C 2015, 119, 15749−15754

field emission scanning electron microscope operating at 10–20 kV is utilized to obtain high-resolution micrographs of the biomorph sheets. The elemental composition of the crystal aggregates is determined using an EDAX Apollo XPP SDD detector. In addition, we conduct atomic force microscopy using an MFP-3D Asylum Research AFM coupled to an ARC2 controller. The topographic images are acquired at a scan rate of 0.25 Hz from 10 × 10 μm^2 regions on the biomorph sheet surface. These measurements are performed in the intermittent contact mode using aluminum-coated AC160TS-R3 Olympus tips. The sheet thickness and roughness data are then analyzed with the help of Igor Pro software.

RESULTS AND DISCUSSION

Figure 1 shows optical micrographs of typical biomorphs that nucleate (a) close to the solution–air interface and (b) on a glass surface in the reaction medium. Despite some minor morphological differences, the biomorphs consist of globular structures surrounded by thin sheets. In the early growth stages, the globules form by the successive branching of carbonate crystallites according to the well-established rod–fractal-dumbbell pathway.[16,33] In contrast to other systems that cease crystal growth at this stage, the silica–carbonate reaction subsequently assembles the striking sheets shown in Figure 1a,b. These structures emerge from the globules and typically adopt cardioid-like shapes with diameters ranging from 10 to 300 μm. Notice that the crystal aggregates near the solution–air interface develop radial structures reminiscent of flower petals (Figure 1a).

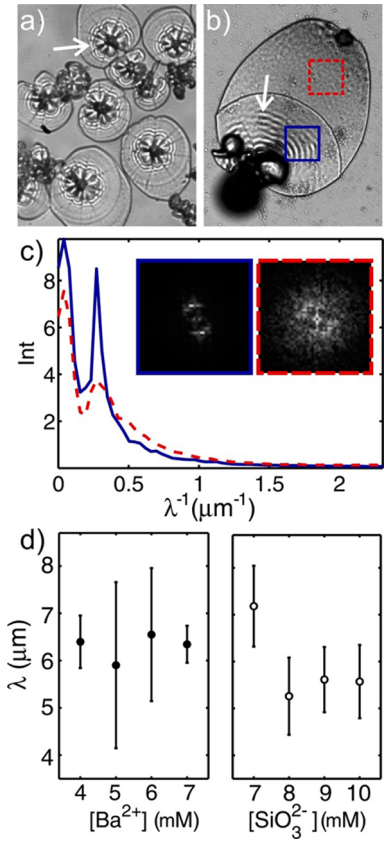

Figure 1. Optical microscopy images of biomorph aggregates at (a) the liquid–air interface and (b) the growth substrate. White arrows highlight the oscillatory patterns that form on the sheet structures. Field of view: (a) 280 × 350 and (b) 130 × 160 μm^2. The blue and red boxes indicate the regions selected for Fourier analysis. (c) Power spectra of the corresponding sheet patterns. (d) Plots showing the effect of varying $[Ba^{2+}]$ at $[SiO_3^{2-}]$ = 8.4 mM (filled circles) and $[SiO_3^{2-}]$ at $[Ba^{2+}]$ = 5 mM (open circles).

Both types of biomorph leaves display stripe patterns. These nearly concentric bands are particularly obvious near the globules from which the sheets originate (arrows in Figure 1a,b) and typically decrease in intensity with increasing distance from the globules. The stripes are not externally templated by the nucleation surface, but represent an inherent morphological characteristic of the biomorph leaves. In addition, these features do not qualitatively change when observed through optical bandpass filters, thus disproving the possibility of optical interference effects such as Newton's rings. With increasing distance from the globule, the ordered bands (Figure 1b, solid, blue box) occasionally transition to disordered patterns reminiscent of coarse laser speckles (dashed, red box). We conduct Fourier transforms on selected 26 × 26 μm^2 areas for these two types of patterns. The corresponding power spectra reflect the directional preference of the oscillatory stripes and the approximate isotropy of the patchy region (Figure 1c, insets). Note that the analysis yields an identical wavelength of about 3.7 μm for both regions. Furthermore, we analyze the biomorph sheet patterns obtained at different reactant concentrations. Figure 1d shows that changing the barium (filled circles) and silicate concentrations (open circles) does not produce an appreciable trend in the average wavelength. We conclude that the characteristic wavelength is largely independent from the pattern type and the initial bulk concentrations.

We monitor the growth dynamics of the crystal aggregates using time-lapse optical microscopy. The biomorph sheets begin to develop after an induction period of approximately 3 h. Figure 2 shows the sheets (a) at an intermediate growth stage

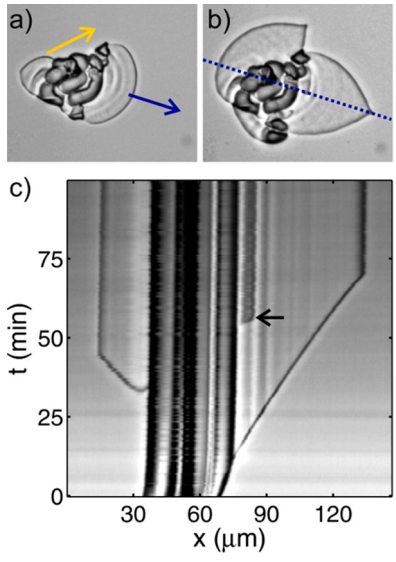

Figure 2. Optical micrographs of (a) an expanding biomorph and (b) the same structure after 50 min. The arrows indicate the growth direction of the two sheets. Field of view: 135 × 110 μm^2. (c) Space-time plot of the biomorph growth constructed by extracting one-dimensional intensity profiles (blue, dotted line) from successive images. The arrow highlights the emergence of a second thin sheet from the crystalline globule.

DOI: 10.1021/acs.jpcc.5b04411
J. Phys. Chem. C 2015, 119, 15749–15754

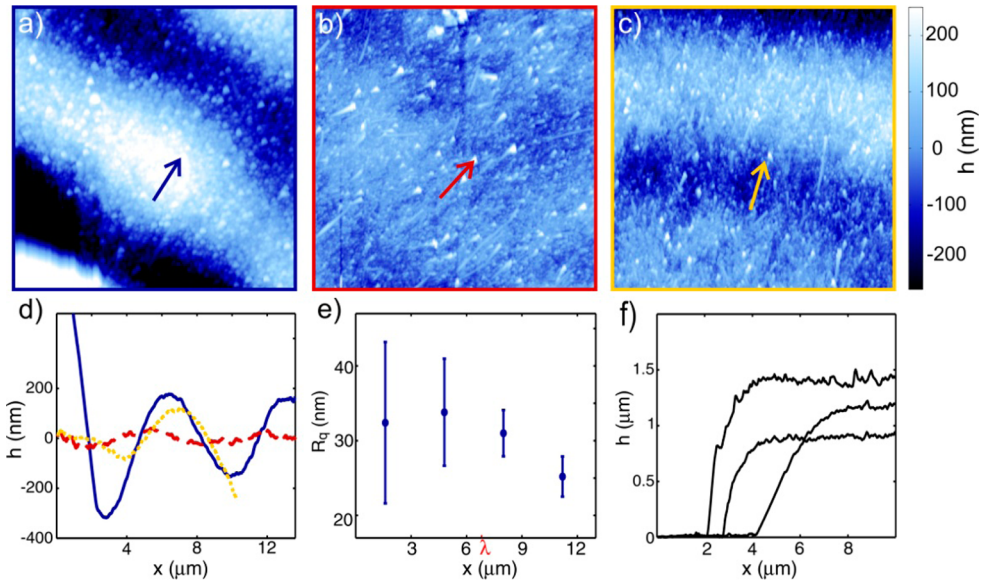

Figure 3. AFM characterization of the surface morphology (a) close to the crystalline globule, (b) in the patchy, middle region, and (c) in the peripheral oscillatory region. Field of view: 10 × 10 μm^2. The arrows indicate the sheet growth direction. (d) Plots of the average amplitude variation in the sheet growth direction. (e) Average local roughness at selected 250 μm^2 areas of the sheet surface. (f) Representative plots of the height difference between the glass substrate and the biomorph surface.

and (b) after the expansion is complete. Earlier studies found that the striking cardioid shapes result from local growth arrest due to a curled-in state of the sheet edge that ultimately terminates the sheet expansion.[28] We observe that the concentric stripes occur parallel to the propagating edge and normal to the growth direction (blue arrow). This finding is obvious for the right sheet in Figure 2 but also holds for the left sheet (see Movie 1 in the Supporting Information).

Further insights into the mesoscopic dynamics can be obtained from the space-time plot in Figure 2c. We construct the plot by stacking one-dimensional intensity profiles from subsequent images of biomorph growth. These profiles are extracted from a constant line across the center of the biomorph (Figure 2b, dotted, blue line). During the expansion, the right sheet front is oriented perpendicular to this line and its cusp occurs only as the sheet expansion ends (approximately after 1 h). Accordingly, the edge of the right sheet appears as a rightwards propagating front and its slope is the inverse growth speed in normal direction to the crystallization edge. The oscillatory stripes occur as vertical bands of constant width and remain stationary throughout the experiment. Most importantly, the stripes form in the immediate wake of the front (or at least within the first 30 s). These findings rule out the possibility of stripe formation due to the delayed deposition of secondary crystals and/or physical buckling instabilities which frequently occur in soft materials.[34,35] However, our results are consistent with the existence of chemical oscillations in close vicinity to the propagating crystallization front.

The normal front velocity of the sheet in Figure 2c accelerates only slightly and averages 0.98 μm/min which is in agreement with values reported earlier.[28,31] This measurement allows us to determine the period of stripe formation and hence the period of the possible concentration oscillations. Considering the average stripe distance of 6.3 ± 0.5 μm, we find a period of approximately 6.4 min. Within the resolution of our measurements, we surprisingly detect no evidence for oscillations in the growth speed. The lack of front oscillations has been commented upon by others[28] but is in our opinion still perplexing.

The space-time plot provides additional information regarding the physical nature of the band patterns. Notice that a second deposition layer emerges from the globule approximately 45 min after the nucleation of the first sheet (Figure 2c, arrow). This secondary layer does not grow to a full-sized leaf but traces one of the stripes in the original sheet. Our observation suggests that the stripes affect the biomorph surface. We hence probe the surface morphology using atomic force microscopy (AFM). Parts a−c of Figure 3 show topographic maps from three sheet regions at increasing distances from the crystalline globule. Bright and dark colors correspond to high and low surface elevations, respectively (see scale bar). The highest points are within the small triangular domain in the lower, left corner of part a, which represents the globule edge. The diagonal bands in part a correspond to the innermost stripes in the optical micrographs. The map in Figure 3b is measured within a spatially disordered, patchy region similar to the one shown in Figure 1b (dashed, red box). In this particular sample, stripes reemerged near the periphery of the biomorph sheet causing correlated height variations (Figure 3c). Despite the large area covered by our AFM measurements (100 μm^2), we resolve some of the much smaller barium carbonate nanorods.

The AFM measurements allow us to quantify the amplitude of the height oscillations. For this purpose, we collapse the topographic maps into average height profiles along the growth direction (Figure 3d). For the representative examples in Figure 3a−c, we find periodic height variations of 350−500 nm in the oscillatory regions (solid, blue and dotted, yellow curves) and approximately 60 nm for the patchy pattern (dashed, red curve). The average wavelength measures 6.6 ± 0.4 μm, which is consistent with our optical data. In the following, we evaluate the significance of the oscillation amplitudes by comparing our measurements to the local surface roughness and the total sheet thickness.

DOI: 10.1021/acs.jpcc.5b04411
J. Phys. Chem. C 2015, 119, 15749−15754

Figure 3e shows the local surface roughness as a function of the distance x from the edge of the globule. The roughness is measured from 500 × 500 nm^2 subsections and fluctuates in an interval of 20−55 nm. These values are an order of magnitude smaller than the oscillation amplitude. Figure 3f shows height profiles across the edges of three biomorph sheets (see also Figures S1 and S2). The average thickness measures 1.1 ± 0.2 μm and has no systematic dependence on the sheet diameter or the measurement position. Height oscillations in the representative samples were absent at these close distances to the sheet edge. We conclude that the oscillatory height variations constitute 25−55% of the sheet thickness and their mechanistic origin must hence be an essential component of the biomorph growth.

The large amplitudes of the observed height variations raise the question if the oscillations result from—or at least coincide with—periodic changes in the nanoscopic architecture of the biomorphs. Earlier studies have established that biomorph sheets consist mainly of dense assemblies of crystalline barium carbonate (witherite) nanorods.[22,25] Electron microscopy, microfocus X-ray diffraction, and polarized optical microscopy revealed that the nanorods are aligned in the radial direction.[22] Parts a−c of Figure 4 show images of the sheet surface obtained by field-emission scanning electron microscopy (FE-SEM). The micrographs strongly suggest that the nanorods are aligned parallel to the average sheet plane in the valleys but protrude out of the plane near the maxima (Figure 4a,b). In addition, we find that the nanorod diameter is highly consistent and measures 52 ± 5 nm (Figure 4c) which is comparable to the local roughness of the biomorph surface. The observed oscillations in nanorod alignment and sheet heights are surprisingly not accompanied by periodic compositional variations. Figure 4d shows the molar percentage of barium carbonate (solid circles) and silica (open circles) as measured by energy dispersive spectroscopy (EDS). The data span a length of more than two wavelengths but show no indication of compositional oscillations.

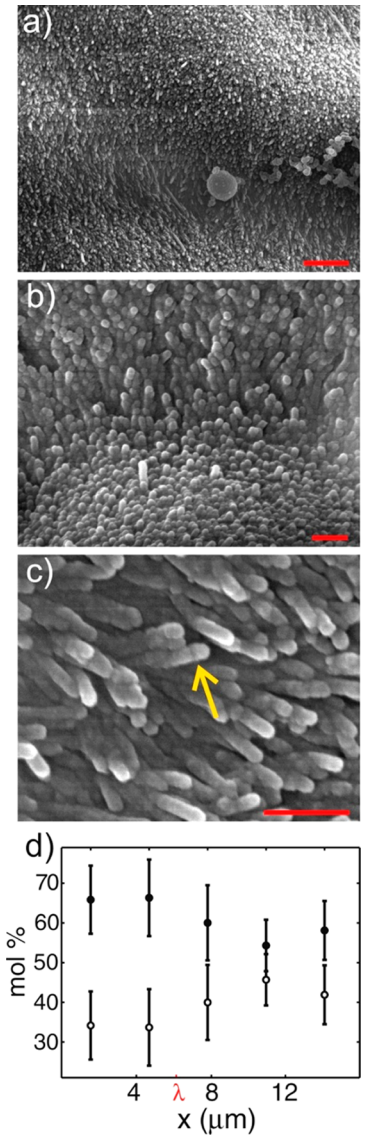

Figure 4. FE-SEM images of nanoscale features on the biomorph leaves. Scale bars represent (a) 1 μm, (b) 300 nm, and (c) 100 nm. (d) Plot of the percent molar composition of barium carbonate (filled circles) and silica (open circles) at increasing distances from the crystalline globule.

CONCLUSIONS

Our study provides the first direct experimental evidence for oscillatory phenomena during the growth of biomorph sheets. We specifically report the existence of large amplitude height variations that take the shape of nearly concentric stripes or disordered patchy patterns with essentially identical wavelengths. These topographic structures correlate with directional variations in the nanorod alignment tilting them periodically out of the average sheet plane. Our results can be discussed in the context of an earlier proposed mechanism for biomorph growth. This model predicts the alternating precipitation of silica and barium carbonate as a central part of pH oscillations at the expanding sheet front. In each iteration of this cyclic process, the deposition of amorphous silica limits the barium carbonate structures to nanorods, thus preventing them from growing into larger euhedral witherite crystals.[32]

Our results show that the topographic patterns form in the immediate wake of the crystallization front which is in agreement with the pH oscillation model. In addition, the stripes are parallel to the growing front suggesting a spatial synchronization of these oscillations. In this context, one can interpret the patchy patterns as desynchronized states with similar frequency and wavelength that lack long-range, lateral correlation. Interestingly, we occasionally observe line defects in the stripe structures that separate synchronized but phase-shifted band patterns (Figure S3). These patterns might present another dynamic state of the oscillatory system. Despite this supporting evidence for chemical oscillations, there remain open questions and some potential contradictions. Foremost, our data show no compositional variations that would be expected from spatiotemporal changes in the production of barium carbonate and silica. Furthermore, the pattern wavelength shows no appreciable dependence on the reactant concentrations. We also do not observe oscillatory changes in the front speed.

These seeming contradictions might be explainable in terms of more complex mechanistic features. Recent studies have reported the formation of prenucleation clusters during the crystallization of alkaline earth metal carbonates in the presence of polyanionic species.[16,36−39] Similar interactions between the silicate oligomers and barium ions can possibly assemble prenucleation clusters during the biomorph crystallization. In this context, the deposition of silica and barium carbonate are

DOI: 10.1021/acs.jpcc.5b04411
J. Phys. Chem. C 2015, 119, 15749−15754

not simply coupled by indirect pH changes, but must be considered as a cocrystallization process.

Regardless of the validity of the pH oscillation model, one can raise the question why the observed nanorods tilt out of the sheet plane. One plausible explanation are variations in the rate of nanorod nucleation and/or termination that intermittently induce overcrowding and force directional adjustments. A similar process might explain the front arrest due to the reported curling and self-trapping of the sheet edge that gives rise to the familiar cardioid leaves and helices. A periodic change in the nucleation-termination balance is also supported by occasional observations of expanding biomorphs that alternate between thin sheets and thick globule-like segments (see Movie 2). These exceptions could be understood as extreme cases of the typical topographical oscillations.

Another unresolved issue is how the growing biomorphs select and maintain their average thickness. Using reliable AFM measurements, our study reports this value as 1.1 μm for substrate-bound sheets. As noted in the literature, the preferential direction for nanorod growth is along the *c*-axis, which introduces a bias for flat sheets.[22,25,28] In addition, symmetry breaking occurs due to the planar substrate surface (which also provides ample nucleation sites). These factors as well as fluctuations and nanorod defects must be considered in a complete description of the basic and oscillatory growth processes. It is less clear in how far diffusion plays a critical role in this system but relaxation oscillations could also occur from the interplay of diffusive transport and thickness-dependent production and consumption at the front. The goal for future studies should be to perform more quantitative measurements of the local concentration fields[40] and ultimately develop a rigorous description capable of reproducing the results reported here.

■ ASSOCIATED CONTENT

Supporting Information

Additional electron microscopy images of the biomorph sheets, AFM images from which the sheet thickness measurements are obtained, optical micrographs, and time-lapse microscopy images of sheet growth. The Supporting Information is available free of charge on the ACS Publications website at DOI: 10.1021/acs.jpcc.5b04411.

■ AUTHOR INFORMATION

Corresponding Author

*(O.S.) E-mail: steinbck@chem.fsu.edu.

Notes

The authors declare no competing financial interest.

■ ACKNOWLEDGMENTS

This work was supported by the National Science Foundation under Grants No. 1005861 and 1213259. The Applied Superconductivity Center at the National High Magnetic Field Laboratory (ASC-NHMFL) provided access to the FE-SEM facility. We thank the Condensed Matter and Material Physics (CMMP) User Facility at the Florida State University for providing access to the SEM and EDS instruments. E.N. acknowledges the Mineralogical Society of America (MSA) and the International Centre for Diffraction Data (ICDD).

■ REFERENCES

(1) Grzybowski, B. A. *Chemistry in Motion: Reaction-Diffusion Systems for Micro- and Nanotechnology*; John Wiley and Sons: Chichester, U.K., 2009.

(2) Liu, Y.; Yuan, W.; Shi, Y.; Chen, X.; Wang, Y.; Chen, H.; Li, H. Functionalizing Single Crystals: Incorporation of Nanoparticles inside Gel-Grown Calcite Crystals. *Angew. Chem., Int. Ed.* **2014**, *53*, 4127−4131.

(3) Makki, R.; Al-Humiari, M.; Dutta, S.; Steinbock, O. Hollow Microtubes and Shells from Reactant-Loaded Polymer Beads. *Angew. Chem., Int. Ed.* **2009**, *48*, 8752−8756.

(4) Makki, R.; Steinbock, O. Nonequilibrium Synthesis of Silica-Supported Magnetite Tubes and Mechanical Control of Their Magnetic Properties. *J. Am. Chem. Soc.* **2012**, *134*, 15519−15527.

(5) Makki, R.; Ji, X.; Mettoussi, H.; Steinbock, O. Self-Organized Tubular Structures as Platforms for Quantum Dots. *J. Am. Chem. Soc.* **2014**, *136*, 6463−6469.

(6) Estroff, L. A.; Hamilton, A. D. At the Interface of Organic and Inorganic Chemistry: Bioinspired Synthesis of Composite Materials. *Chem. Mater.* **2001**, *13*, 3227−3235.

(7) Li, H.; Estroff, L. A. Calcite Growth in Hydrogels: Assessing the Mechanism of Polymer-Network Incorporation into Single Crystals. *Adv. Mater.* **2009**, *21*, 470−473.

(8) Asenath-Smith, E.; Li, H.; Keene, E. C.; Seh, Z. W.; Estroff, L. A. Crystal Growth of Calcium Carbonate in Hydrogels as a Model of Biomineralization. *Adv. Funct. Mater.* **2012**, *22*, 2891−2914.

(9) Lim, B.; Jiang, M.; Camargo, P. H.; Cho, E. C.; Tao, J.; Lu, X.; Zhu, Y.; Xia, Y. Pd-Pt Bimetallic Nanodendrites with High Activity for Oxygen Reduction. *Science* **2009**, *324*, 1302−1305.

(10) Mohanty, A.; Garg, N.; Jin, R. A Universal Approach to the Synthesis of Noble Metal Nanodendrites and Their Catalytic Properties. *Angew. Chem., Int. Ed.* **2010**, *49*, 4962−4966.

(11) Fournier-Bidoz, S.; Arsenault, A. C.; Manners, I.; Ozin, G. A. Synthetic Self-Propelled Nanorotors. *Chem. Commun.* **2005**, *4*, 441−443.

(12) Maselko, J.; Borisova, P.; Carnahan, M.; Dreyer, E.; Devon, R.; Schmoll, M.; Douthat, D. Spontaneous Formation of Chemical Motors in Simple Inorganic Systems. *J. Mater. Sci.* **2005**, *40*, 4671−4673.

(13) White, S. R.; Sottos, N. R.; Geubelle, P. H.; Moore, J. S.; Kessler, M. R.; Sriram, S. R.; Brown, E. N.; Viswanathan, S. Autonomic Healing of Polymer Composites. *Nature* **2001**, *409*, 794−797.

(14) Blaiszik, B. J.; Kramer, S. L. B.; Olugebefola, S. C.; Moore, J. S.; Sottos, N. R.; White, S. R. Self-Healing Polymers and Composites. *Annu. Rev. Mater. Res.* **2010**, *40*, 179−211.

(15) Mann, S. *Biomineralization: Principles and Concepts in Bioinorganic Materials Chemistry*; Oxford Chemistry Masters; Oxford University Press: Oxford, U.K., 2001.

(16) Cölfen, H.; Antonietti, M. *Mesocrystals and Nonclassical Crystallization*; John Wiley & Sons, Ltd.: Chichester, U.K., 2008.

(17) Zhou, L.; O'Brien, P. Mesocrystals — Properties and Applications. *J. Phys. Chem. Lett.* **2012**, *3*, 620−628.

(18) Balasz, A. C.; Bhattacharya, A.; Tripathi, A.; Shum, S. Designing Bioinspired Artificial Cilia to Regulate Particle−Surface Interactions. *J. Phys. Chem. Lett.* **2014**, *5*, 1691−1700.

(19) Voinescu, A. E.; Kellermeier, M.; Carnerup, A. M.; Larsson, A.-K.; Touraud, D.; Hyde, S. T.; Kunz, W. Co-Precipitation of Silica and Alkaline-Earth Carbonates Using TEOS as Silica Source. *J. Cryst. Growth* **2007**, *306*, 152−158.

(20) García-Ruiz, J. M.; Melero-García, E.; Hyde, S. T. Morphogenesis of Self-Assembled Nanocrystalline Materials of Barium Carbonate and Silica. *Science* **2009**, *323*, 362−365.

(21) Bittarello, E.; Massaro, F. R.; Aquilano, D. The Epitaxial Role of Silica Groups in Promoting the Formation of Silica/Carbonate Biomorphs: A First Hypothesis. *J. Cryst. Growth* **2010**, *312*, 402−412.

(22) Kellermeier, M.; Cölfen, H.; García-Ruiz, J. M. Silica Biomorphs: Complex Biomimetic Hybrid Materials from "Sand and Chalk". *Eur. J. Inorg. Chem.* **2012**, *32*, 5123−5144.

(23) Kellermeier, M.; Eiblmeier, J.; Melero-García, E.; Pretzl, M.; Fery, A.; Kunz, W. Evolution and Control of Complex Curved Form in

DOI: 10.1021/acs.jpcc.5b04411
J. Phys. Chem. C 2015, 119, 15749−15754

Simple Inorganic Precipitation Systems. *Cryst. Growth Des.* **2012**, *12*, 3647−3655.
(24) Sanchez-Puig, N.; Guerra-Flores, E.; Lopez-Sanchez, F.; Juarez-Espinoza, P. A.; Ruiz-Arellano, R.; Gonzalez-Munoz, R.; Arreguin-Espinosa, R.; Moreno, A. Controlling the Morphology of Silica-Carbonate Biomorphs Using Proteins Involved in Biomineralization. *J. Mater. Sci.* **2012**, *47*, 2943−2950.
(25) García-Ruiz, J. M.; Hyde, S. T.; Carnerup, A. M.; Christy, A. G.; Van Kranendonk, M. J.; Welhalm, N. J. Self-Assembled Silica-Carbonate Structures and Detection of Ancient Microfossils. *Science* **2003**, *202*, 1194−1197.
(26) Hyde, S. T.; Carnerup, A. M.; Larsson, A.-K.; Christy, A. G.; García-Ruiz, J. M. Self-Assembly of Carbonate-Silica Colloids: Between Living and Non-Living Form. *Physica A* **2004**, *339*, 24−33.
(27) Kunz, W.; Kellermeier, M. Beyond Biomineralization. *Science* **2009**, *323*, 344−345.
(28) García-Ruiz, J. M.; Melero-García, E.; Hyde, S. T. Morphogenesis of Self-Assembled Nanocrystalline Materials of Barium Carbonate and Silica. *Science* **2009**, *323*, 362−365.
(29) Wilson, M. Oscillating Chemistry Explains Complex, Self-Assembled Crystal Aggregates. *Phys. Today* **2009**, *62*, 17−18.
(30) Kellermeier, M.; Melero-García, E.; Kunz, W.; García-Ruiz. Local Autocatalytic Co-Precipitation Phenomena in Self-Assembled Silica−Carbonate Materials. *J. Colloid Interface Sci.* **2012**, *380*, 1−7.
(31) Kellermeier, M.; Melero-García, E.; Glaab, F.; Eiblmeier, J.; Kienle, L.; Rachel, R.; Kunz, W.; García-Ruiz, J. M. Growth Behavior and Kinetics of Self-Assembled Silica−Carbonate Biomorphs. *Chem.−Eur. J.* **2012**, *18*, 2272−2282.
(32) Eiblmeier, J.; Schürmann, U.; Kienle, L.; Gebauer, D.; Kunz, W.; Kellermeier, M. New Insights into the Early Stages of Silica-Controlled Barium Carbonate Crystallisation. *Nanoscale* **2014**, *6*, 14939−14949.
(33) Busch, S.; Dolhaine, H.; DuChesne, A.; Heinz, S.; Hochrein, O.; Laeri, F.; Podebrad, O.; Vietze, U.; Weiland, T.; Kniep, R. Biomimetic Morphogenesis of Fluorapatite-Gelatin Composites: Fractal Growth, the Question of Intrinsic Electric Fields, Core/Shell Assemblies, Hollow Spheres and Reorganization of Denatured Collagen. *Eur. J. Inorg. Chem.* **1999**, *10*, 1643−1653.
(34) Edmondson, S.; Frieda, K.; Comrie, J. E.; Onck, P. R.; Huck, W. T. S. Buckling in Quasi-2D Polymers. *Adv. Mater. 18*, 724−728.
(35) Verduzco, R.; Meng, G.; Kornfield, J. A.; Meyer, R. B. Buckling Instability in Liquid Crystalline Physical Gels. *Phys. Rev. Lett.* **2006**, *96*, 147802.
(36) Gower, L. B.; Odom, D. J. Deposition of Calcium Carbonate Films by a Polymer-Induced Liquid-Precursor (PILP) Process. *J. Cryst. Growth* **2000**, *210*, 719−734.
(37) Cheng, X.; Varona, P. L.; Olszta, M. J.; Gower, L. B. Biomimetic Synthesis of Calcite Films by a Polymer-Induced Liquid-Precursor (PILP) Process. *J. Cryst. Growth* **2007**, *307*, 395−404.
(38) Homeijer, S. J.; Barrett, R. A.; Gower, L. B. Polymer-Induced Liquid-Precursor (PILP) Process in the Non-Calcium Based Systems of Barium and Strontium Carbonate. *Cryst. Growth Des.* **2010**, *10*, 1040−1052.
(39) Gebauer, D.; Kellermeier, M.; Gale, J. D.; Bergström, L.; Cölfen, H. Pre-Nucleation Clusters as Solute Precursors in Crystallisation. *Chem. Soc. Rev.* **2014**, *43*, 2348−2371.
(40) Ibaraki, S.; Ise, R.; Ishimori, K.; Oaki, Y.; Sazaki, G.; Yokoyama, E.; Tsukamotode, K.; Imai, H. Oscillatory Growth for Twisting Crystals. *Chem. Commun.* **2015**, *51*, 8516−8519.

DOI: 10.1021/acs.jpcc.5b04411
J. Phys. Chem. C 2015, 119, 15749−15754